JACS
JOURNAL OF THE AMERICAN CHEMICAL SOCIETY

Communication

pubs.acs.org/JACS

Mesoporous TiO_2 Nanocrystals Grown in Situ on Graphene Aerogels for High Photocatalysis and Lithium-Ion Batteries

Bocheng Qiu, Mingyang Xing,* and Jinlong Zhang*

Key Laboratory for Advanced Materials and Institute of Fine Chemicals, East China University of Science and Technology, 130 Meilong Road, Shanghai 200237, P.R. China

Supporting Information

ABSTRACT: TiO_2/graphene composites have been well studied as a solar light photocatalysts and electrode materials for lithium-ion batteries (LIBs). Recent reports have shown that ultralight 3D-graphene aerogels (GAs) can better adsorb organic pollutants and can provide multidimensional electron transport pathways, implying a significant potential application for photocatalysis and LIBs. Here, we report a simple one-step hydrothermal method toward in situ growth of ultradispersed mesoporous TiO_2 nanocrystals with (001) facets on GAs. This method uses glucose as the dispersant and linker owing to its hierarchically porous structure and a high surface area. The TiO_2/GAs reported here exhibit a highly recyclable photocatalytic activity for methyl orange pollutant and a high specific capacity in LIBs. The strong interaction between TiO_2 and GAs, the facet characteristics, the high electrical conductivity, and the three-dimensional hierarchically porous structure of these composites results in highly active photocatalysis, a high rate capability, and stable cycling.

Graphene (GR) has a large specific surface area, excellent conductive, mechanical, and hydrophobic properties and is chemically stabile, making it an ideal support.[1−4] These properties allow it to be a multifunctional material with an excellent capacity for carrying and conducting electrons and holes. Recently, a series of graphene-based materials have attracted great attention,[5] and hybrid systems composed of inorganic nanoparticles have resulted in many promising applications in areas ranging from solar light photocatalysis to Li-ion batteries (LIBs).[4,6−8] In particular, three-dimensional (3D) graphene aerogels (GAs) compounded with TiO_2 composites are ultralight massive catalysts,[9−12] which display hydrophobic properties and facilitate photocatalyst recycling. Compared with 2D graphene, the volumes, shapes, and densities of 3D GAs can be easily controlled by adjusting reaction vessel characteristics, enabling access to large scale production.[11] The hierarchically porous structure of TiO_2/GAs can provide more Li-ion transfer channels,[13] providing an ideal negative electrode material well suited for LIBs. However, one of the biggest problems hindering the application of TiO_2/GAs is the stability of the interaction between TiO_2 nanoparticles and the GA surface.[5,6] As a consequence of the weak interaction between TiO_2 facets and GR surface during the reduction process, in situ growth of ultradispersed TiO_2 nanocrystals on the surface of GR sheets can be difficult to achieve.[14] This is especially true for GAs, as the single macroporous structure is likely to increase the loss of nanoparticles from GR surface. The weak interaction between TiO_2 and GAs may hinder the transfer of electrons and Li ions, impeding application in photocatalysis and LIBs.

We report a simple one-step hydrothermal method for the preparation of ultradispersed TiO_2 single nanocrystals grown in situ on a GA surface. This method uses glucose as the linker and face-controlling agent to produce (001) facets and a mesoporous structure on TiO_2. The resulting TiO_2/GAs have highly recyclable photocatalytic activity, a high rate capability, and stable cycling in LIBs.

To grow the nanocrystals, $Ti(SO_4)_2$ is first dissolved in an aqueous solution to cultivate crystal seeds before a known amount of glucose is adsorbed on the seeds, fixing the seeds on the surface of graphene oxides (GO, Figure 1a).[15] A 3D-structured TiO_2/GA (with a density of 19 mg/cm^3) is then prepared by a one-step hydrothermal treatment. During the hydrothermal process, large numbers of glucose molecules adsorb onto the (001) surfaces, generating nanosized seeds with exposed (001) facets owing to many hydroxyl groups on glucose.[15] This process is beneficial for the formation of (001) facets and hinders the aggregation of nanoparticles.[15] The

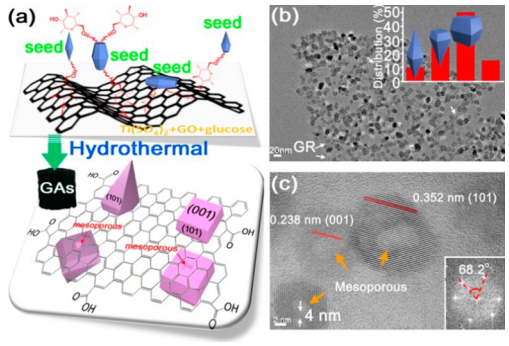

Figure 1. (a) Glucose-linked transformation pathway for the in situ growth of TiO_2 nanocrystals with (001) facets on the GAs surface. (b) TEM image for TiO_2/GAs (67 wt % of TiO_2 in TiO_2/GAs). Inset (b) is the corresponding morphology distribution of the TiO_2 nanocrystals derived from 100 of TiO_2 crystals in image (b). (c) HRTEM image for TiO_2/GAs (67 wt %). Inset (c) is the corresponding fast Fourier transform (FFT) pattern.

Received: January 26, 2014
Published: April 8, 2014

   dx.doi.org/10.1021/ja500873u | J. Am. Chem. Soc. 2014, 136, 5852−5855

presence of glucose results in a percentage of nanocrystals exposed with (001) of up to 50% (inset of Figure 1b) and sizes ranging from 15−20 nm. Interestingly, the interface between TiO_2 facets and the GR surface has a mesoporous structure (Figures 1c and S1a). The light-colored part in the center of TiO_2 nanocrystal is the mesoporous channel with a size of 4−6 nm. There are 3−6 layers of graphene in the TiO_2/GAs and one layer of graphene with a thickness of 0.4−1.0 nm (Figure S1b). Although it is very difficult to obtain monolayer graphene in 3D-GAs, our results show that the conductivity and photocatalytic properties of TiO_2/GAs are far better than those of blank TiO_2 nanocrystals. The HRTEM image also shows the characteristic lattice fringe of (001) and (101) facets (Figure 1c). The corresponding FFT pattern indicates that the TiO_2 is in the form of a single crystal and the angle between (001) and the (101) plane is 68.2°.[16] During the growth of TiO_2, the hydroxyl groups at one end of glucose connect with GR, while the hydroxyl groups at the other end connect with the TiO_2 facets. Thus, the hydroxyl groups enable glucose to serve as the linker enabling the in situ growth of TiO_2 nanocrystals on a GA surface. The glucose adsorbed toward the sides of GR is acting as face-growth inhibitors, slowing the growth of the involved face of TiO_2 and the production of mesoporous channels in the TiO_2 nanocrystals. The surface area of TiO_2/GAs can be up to 204 m^2g^{-1}, exceeding those of some other metal oxides/GAs.[17] The mesoporous structure is expected to improve the adsorption of organic pollutants for photocatalysis and the storage of Li ions in LIBs.[13]

TiO_2/GAs in the absence of glucose were also synthesized (using a similar strategy) in order to investigate the role of glucose in the in situ growth of TiO_2 nanocrystals. The corresponding TEM images are shown in Figures 2a and S1b,c.

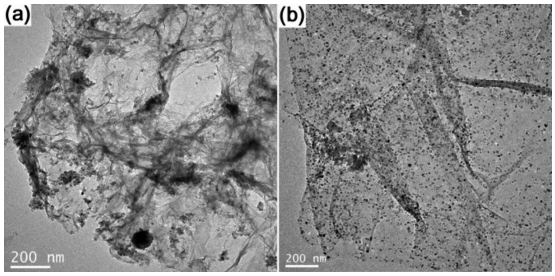

Figure 2. TEM images of TiO_2/GAs (67 wt %) synthesized in the absence (a) or presence (b) of glucose.

Compared with the TiO_2/GAs synthesized in the presence of glucose (Figures 2b and S1d), there is obvious aggregation observable in Figures 2a and S1c, indicating that of the presence of glucose between TiO_2 and GR can immobilize the crystal seeds on GR, enabling the in situ growth of ultradispersed TiO_2 nanocrystals. In the presence of glucose, the theoretical proportion of TiO_2 is 67%, which agrees well with TGA results (64.8% in Figure S2). Although the proportion of TiO_2 increases from 20 to 80 wt %, the distribution of nanocrystals remains ultradispersive (Figure S3), indicating that the in situ growth of TiO_2 is determined by the presence of glucose rather than the concentration of $Ti(SO_4)_2$. The distribution profile of Ti elements in TEM mapping is consistent with the profile of GR sheets (Figure S4), verifying the ultradispersed distribution of TiO_2 nanocrsytals on the GA surface.

As with the microstructure, the macrostructure of TiO_2/GAs also shows an improved appearance. The macrostructure has a light, massive appearance after hydrothermal treatment in an aqueous solution (Figure 3a). The resulting aerogels exhibit

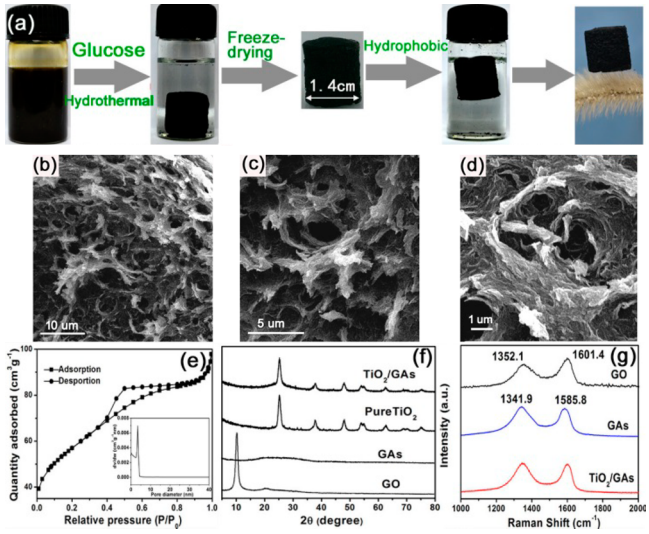

Figure 3. (a) Appearance illustration of TiO_2/GAs involving glucose. (b−d) Low- and high-magnification SEM images of TiO_2/GAs (67 wt %) synthesized in the presence of glucose. (e) Nitrogen adsorption−desorption isotherms of TiO_2/AGs and its corresponding pore size distribution curves (inset). (f) XRD and (g) Raman spectra of different samples.

hydrophobic properties after the freeze-drying treatment, which is expected to allow for the recycling of the catalyst for applications in photocatalysis. Although the TiO_2/GAs exhibit a relative high density compared with the pure GAs, it also can be standing on the dog's tail grass. In addition to the mesoporous structure, the GAs also has a macroporous structure (Figure 3b−d) with pore sizes in the range of 0.1−5 μm. Compared with the SEM image for the sample prepared in the absence of glucose (Figure S5), the TiO_2/GAs maintain the macroporous structure (Figure 3b−d). The compressibility of TiO_2/GAs is displayed in Figure S6. TiO_2/GAs prepared in the presence of glucose unfolds almost completely after removing the external pressure. The results indicate that the addition of glucose cannot destroy the macrostructure and the mechanical strength of TiO_2/GAs. The hierarchical channels are beneficial for the insertion/removal of Li ions and the free adsorption of organic pollutants.[13] The nitrogen adsorption−desorption isotherm of TiO_2/GAs indicates that the GAs possess a typical mesoporous structure and that pore size is mainly in the range of 4−5 nm (Figure 3e), agreeing with HRTEM results (Figure 1c). The XRD results indicate that GO can be reduced to GR by hydrothermal treatment and that the TiO_2 nanocrystals are the anatase crystal structures (Figure 3f). After hydrothermal treatment, the D- and G-bands of the RAMAN spectra at 1352.1 and 1601.4 cm^{-1} shift to 1341.9 and 1585.8 cm^{-1}, respectively, indicating the successfully reduction of GO (Figure 3g).[18] The increase of the intensity ratio of D/G bands after hydrothermal treatment further confirms the reduction of GO (from 0.96 to 1.02).[17]

The solar-driven photocatalytic activity of TiO_2/GAs is measured by monitoring the degradation of methyl orange (MO, 10 mg/L, Figure 4a). After irradiation for 5 h, the MO can be degraded up to 90% by TiO_2/GAs (67 wt %), far exceeding known P25-based GA catalysts (67 wt %). After 5 cycles, the catalyst maintains high photoactivity (83%), while P25/GAs exhibit decreased rates of MO degradation (9.4%). Additionally,

dx.doi.org/10.1021/ja500873u | J. Am. Chem. Soc. 2014, 136, 5852−5855

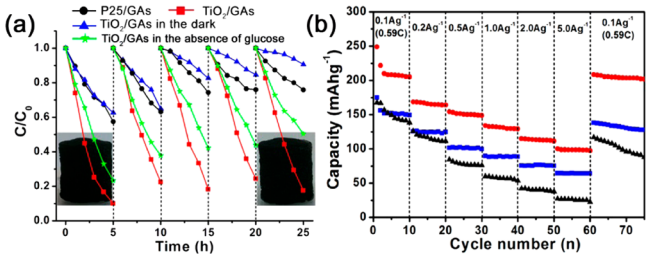

Figure 4. (a) Cycling photodegradation of MO under simulated solar light irradiation (with an AM 1.5 air mass filter). (b) Cycling performance of TiO_2/GAs (red), TiO_2/GAs in the absence of glucose (blue), and pure TiO_2 (black) electrodes at different current densities from 0.1 to 5.0 Ag^{-1}.

when a TiO_2/GA was prepared in the absence of glucose, its photocatalytic activity decreased, and it became unstable (green line in Figure 4a). These results demonstrate the photocatalytic advantage of the ultradispersed and mesoporous structures of the TiO_2/GAs as prepared here. However, TiO_2/GAs has a gradually diminishing adsorption capacity for MO when placed in the dark after 5 cycles (blue lines in Figure 4a). The low density and the massive appearance of TiO_2/GAs enable easy recycling with constant morphology (inset of Figure 4a) and a mass loss of <5% after 5 cycles (Figure S7). Increasing TiO_2 proportions results in a significant increase in the photoactivity of TiO_2/GAs leading to a significant increase in the degradation of MO (Figure S8). When the TiO_2 proportion is increased to 80 wt %, the degradation rate can exceed 90% within 3 h of irradiation. Interestingly, the TiO_2/GAs are always observed to be floating on top of the liquid phase during the photodegradation process (Figure S9a) and can be easily separated for recycling using a tweezer (Figure S9b). A comparison of photocatalytic activity between TiO_2/GAs and black hydrogen-doped TiO_2 has been done to highlight the advantage of TiO_2/GAs.[19−21] A couple of TiO_2/GAs show a little higher photoactivity than the H-TiO_2 in the absence of stirring during the whole photodegradation process (details in Figure S10). The microstructure of TiO_2/GAs maintains an ultradispersed TiO_2 distribution after 5 cycles (Figure S11), indicating that the prepared TiO_2/GAs have a very stable structure. The TiO_2 nanocrystals are firmly fixed on the surface of GAs, owing to a strong interaction between them. This interaction is induced by the linking action of glucose, which is also responsible for the high photocatalytic performance of TiO_2/GAs. In the FTIR spectra of TiO_2/GAs (Figure S12), the appearance of −C−O−C− signals results from the covalent linkage between the hydroxide radicals of GR and glucose. This reaction results in a new and very broad peak in the range of 600−800 cm^{-1} belonging to the resulting Ti−O−C bond,[22] indicating the interaction between the GA and TiO_2 (details in Supporting Information (SI)). The results of C 1s XPS spectra show the reduction of GO (Figure S13, details in SI), and there is a significant shift of C−C peak from 285.0 to 284.6 eV after glucose addition, suggesting that Ti−C bonds have been formed between TiO_2 and GAs. Hence, we can conclude that the interaction between GAs and TiO_2 is built and strengthened by the formation of different chemical bonds, resulting in the in situ growth of TiO_2 nanocrystals on GA surfaces. All the above results indicate the presence of interaction between TiO_2 and GR through a glucose linker. Under solar light irradiation, the photoexcited electrons transfer from the TiO_2 nanocrystals to the GR by a glucose linker (Figure S14), and the holes assemble on the (001) facets, enhancing the separation of electrons and holes.[23] The electrons further react with O_2 to generate the hydroxyl radicals responsible for the observed high photocatalytic activity of TiO_2/GAs.

In addition to this high photocatalytic activity, the TiO_2/GAs also enable the high performance of LIBs. Figure S15 shows the charge−discharge curves of TiO_2/GAs as an anode at a current rate of 0.59 C (0.1 Ag^{-1}). The horizontal discharge plateau is at 1.76 V, and the horizontal charge plateau is at 1.95 eV, which are characteristic of lithium insertion/extraction between TiO_2 nanocrystals and $Li_{0.5}TiO_2$.[6] It has been demonstrated that ordinary anatase TiO_2 gives only the orthorhombic $Li_{0.5}TiO_2$ (the conventional definition form of theoretical lithium capacity of TiO_2). The cubic $LiTiO_2$ with a higher lithium storage capacity can indeed be formed in nanostructured TiO_2 as a result of quantum-size confinement effect.[14,24] The slope below 1.76 is characteristic of capacitive behavior and results from the excellent storage of lithium ions owing to the presence of a mesoporous structure. The change in the plateau potential of the TiO_2/GAs electrode is very small owing to its high conductivity. As a result, a high capacity of 605 $mAhg^{-1}$ can be delivered in the first discharge, much higher than other reported TiO_2/carbon electrodes.[6,25−29] Recently, Zhao et al.[6] developed a sol−gel design strategy toward ultradispersed TiO_2 nanoparticles on 2D graphene for high performance LIBs. The capacity of these materials can be up to 352 $mAhg^{-1}$ in the first discharge at 0.59 C.

Liu et al.[30−33] have extensively investigated the electrochemical properties of carbon-based materials. For example, they successfully prepared 3D TiO_2/carbon materials and found that in the voltage range of 3.0−0.05 V vs Li^+/Li, the total first discharge capacity of the hybrid electrode can be up to 648.7 $mAhg^{-1}$,[30] still lower than the 956.2 $mAhg^{-1}$ of the TiO_2/GAs prepared here (inset of Figure S15, voltage range of 3.0−0.05 V). Compare with 2D-structured TiO_2/GRs and some other TiO_2/carbon materials, our TiO_2 nanocrystals grown in situ on 3D-structured GAs have a hierarchically porous structure. This feature is beneficial for lithium insertion/extraction and the storage of lithium ions. Figure S16 shows the cycling performance of different electrodes at constant current densities of 0.59 C. It is clear that the TiO_2/GAs electrode shows a much higher capacity and much more stable capacity than the blank TiO_2 electrode. It still possesses an excellent capacity of 200 $mAhg^{-1}$ after 50 cycles. Figure 4b is the cycling performance compared among TiO_2/GAs prepared with and without glucose and blank TiO_2 electrodes. Remarkably, even when only 67 wt % of the ingredient is active, a reversible capacity of 99 $mAhg^{-1}$ can still be delivered at a very high rate of 5000 mAg^{-1}, which is 4 times higher than that of the pure TiO_2 nanocrystals. When glucose is absent in TiO_2/GAs, the capacity of the material decreases significantly but remains higher than pure TiO_2 (Figure 4b of blue line). In the absence of glucose, the TiO_2/GAs shows a low dispersion of TiO_2 nanocrystals and an absence of mesoporous structure, hindering the transfer of electrons and the storage of Li ions. Importantly, after the high current density measurements, the capacity of the TiO_2 /GAs at 0.59 C can recover to the initial value of 202 $mAhg^{-1}$, suggesting high reversibility. TiO_2/GAs (67 wt %) exhibits the highest capacity in all the samples (Figure S17). When the proportion of TiO_2 in TiO_2/GAs is increase to 80 wt %, the capacity significantly decreases. This observation means that higher proportions of TiO_2 are beneficial to the photoactivity but limits application in LIBs. This may be explained by the fact that excessive, tightly packed TiO_2 nanocrystals prevent the insertion of Li^+. A solution is to amplify the volume of GAs by adjusting the reaction vessel,[11] which is

dx.doi.org/10.1021/ja500873u | J. Am. Chem. Soc. 2014, 136, 5852−5855

expected to enhance the dispersion of TiO_2 nanocrystals on GA surfaces. Moreover, the cycle stabilities of TiO_2/GAs at high rates are indicative of the ultrafast diffusion of lithium ions in bulk, owing to the mesoporous structure, and the short diffusion path length and stability of the 3D graphene structure. Figure S18 compares the Nyquist plots of different electrodes. The TiO_2/GAs electrode has a much lower resistance than the pure TiO_2 electrode (65 vs 136 Ω), owing to the highly conductive GAs that facilitates electron transfer from anchored TiO_2 nanocrystals within the whole electrode.

Therefore, the in situ growth of TiO_2 nanocrystals on GAs can control the size of single crystals and provide an ultradispersed distribution of nanocrystals, affording strong interactions between TiO_2 and GAs and a short diffusion distances for lithium-insertion/extraction (Figure S19). The exposure of (001) facets and the strong connection between TiO_2 and GR improve the electron transport efficiency and provide a stable charge/discharge process, resulting in the observed high rate and cycling stability of TiO_2/GAs. It is worth mentioning that the mesoporous structures on TiO_2 nanocrystals are beneficial for the storage of Li ions, improving the reversible capacity of TiO_2/GAs.

In conclusion, we use a one-step hydrothermal method to prepare 3D-structured TiO_2/GA composites. Glucose is used as the facet-controlling agent and the connection linker to successfully achieve in situ growth of TiO_2 nanocrystals on GAs surfaces. TiO_2 nanocrystals exposed with (001) facets and mesoporous structure are highly dispersed on the GAs surface, affording the high surface area, massive appearance, and hydrophobic properties which determine its highly recyclable photoactivity. This 3D-structured photocatalyst has great potential application for air purification. Further, these materials exhibit excellent specific capacity, outstanding lithium storage performance, highly reversible capacity, and excellent rate performance. We believe that the present synthetic route can be further extended to produce other in situ growth metal oxide/carbon hybrid materials with promising applications for photocatalysis, supercapacitors, and fuel cells.

■ ASSOCIATED CONTENT

Ⓢ Supporting Information

Experimental procedures and characterization details. This material is available free of charge via the Internet at http://pubs.acs.org.

■ AUTHOR INFORMATION

Corresponding Author

mingyangxing@ecust.edu.cn; jlzhang@ecust.edu.cn

Notes

The authors declare no competing financial interest.

■ ACKNOWLEDGMENTS

This work has been supported by National Nature Science Foundation of China (2013CB632403, 21237003, 21073060, 21203062), National Basic Research Program of China (973 Program, 2010CB732306, 2011CB808505), the Project of International Cooperation of the Ministry of Science and Technology of China (2011DFA50530), the Science and Technology Commission of Shanghai Municipality (12230705000) and sponsored by the Program of Shanghai Subject Chief Scientist (12XD1402200) and the Fundamental Research Funds for the Central Universities.

■ REFERENCES

(1) Geim, A. K. *Science* **2009**, *324*, 1530.
(2) Ponomarenko, L. A.; Schedin, F.; Katsnelson, M. I.; Yang, R.; Hill, E. W.; Novoselov, K. S.; Geim, A. K. *Science* **2008**, *320*, 356.
(3) Wang, H.; Robinson, J. T.; Li, X.; Dai, H. *J. Am. Chem. Soc.* **2009**, *131*, 9910.
(4) Xiang, Q.; Yu, J.; Jaroniec, M. *J. Am. Chem. Soc.* **2012**, *134*, 6575.
(5) Li, D.; Kaner, R. B. *Science* **2008**, *320*, 1170.
(6) Li, W.; Wang, F.; Feng, S.; Wang, J.; Sun, Z.; Li, B.; Li, Y.; Yang, J.; Elzatahry, A. A.; Xia, Y.; Zhao, D. *J. Am. Chem. Soc.* **2013**, *135*, 18300.
(7) Zhang, H.; Lv, X.; Li, Y.; Wang, Y.; Li, J. *ACS Nano* **2009**, *4*, 380.
(8) Wu, Z.-S.; Winter, A.; Chen, L.; Sun, Y.; Turchanin, A.; Feng, X.; Müllen, K. *Adv. Mater.* **2012**, *24*, 5130.
(9) Wu, Z.-Y.; Li, C.; Liang, H.-W.; Chen, J.-F.; Yu, S.-H. *Angew. Chem., Int. Ed.* **2013**, *52*, 2925.
(10) Hu, H.; Zhao, Z.; Wan, W.; Gogotsi, Y.; Qiu, J. *Adv. Mater.* **2013**, *25*, 2219.
(11) Sun, H.; Xu, Z.; Gao, C. *Adv. Mater.* **2013**, *25*, 2554.
(12) Zhao, Y.; Hu, C.; Hu, Y.; Cheng, H.; Shi, G.; Qu, L. *Angew. Chem., Int. Ed.* **2012**, *51*, 11371.
(13) Huang, Y.; Wu, D.; Han, S.; Li, S.; Xiao, L.; Zhang, F.; Feng, X. *ChemSusChem* **2013**, *6*, 1510.
(14) Mo, R.; Lei, Z.; Sun, K.; Rooney, D. *Adv. Mater.* **2014**, *26*, 2084.
(15) Xing, M. Y.; Qi, D. Y.; Zhang, J. L.; Chen, F. *Chem.—Eur. J.* **2011**, *17*, 11432.
(16) Xing, M.-Y.; Yang, B.-X.; Yu, H.; Tian, B.-Z.; Bagwasi, S.; Zhang, J.-L.; Gong, X.-Q. *J. Phys. Chem. Lett.* **2013**, *4*, 3910.
(17) Xiao, L.; Wu, D.; Han, S.; Huang, Y.; Li, S.; He, M.; Zhang, F.; Feng, X. *ACS Appl. Mater. Interfaces* **2013**, *5*, 3764.
(18) Xiang, Q.; Yu, J.; Jaroniec, M. *Nanoscale* **2011**, *3*, 3670.
(19) Chen, X.; Liu, L.; Yu, P. Y.; Mao, S. S. *Science* **2011**, *331*, 746.
(20) Naldoni, A.; Allieta, M.; Santangelo, S.; Marelli, M.; Fabbri, F.; Cappelli, S.; Bianchi, C. L.; Psaro, R.; Dal Santo, V. *J. Am. Chem. Soc.* **2012**, *134*, 7600.
(21) Wang, Z.; Yang, C.; Lin, T.; Yin, H.; Chen, P.; Wan, D.; Xu, F.; Huang, F.; Lin, J.; Xie, X.; Jiang, M. *Adv. Funct. Mater.* **2013**, *23*, 5444.
(22) Sakthivel, S.; Kisch, H. *Angew. Chem., Int. Ed.* **2003**, *42*, 4908.
(23) Tachikawa, T.; Yamashita, S.; Majima, T. *J. Am. Chem. Soc.* **2011**, *133*, 7197.
(24) Kavan, L.; Kalbáč, M.; Zukalová, M.; Exnar, I.; Lorenzen, V.; Nesper, R.; Graetzel, M. *Chem. Mater.* **2004**, *16*, 477.
(25) Wang, D.; Choi, D.; Li, J.; Yang, Z.; Nie, Z.; Kou, R.; Hu, D.; Wang, C.; Saraf, L. V.; Zhang, J.; Aksay, I. A.; Liu, J. *ACS Nano* **2009**, *3*, 907.
(26) Xin, X.; Zhou, X.; Wu, J.; Yao, X.; Liu, Z. *ACS Nano* **2012**, *6*, 11035.
(27) Ren, Y.; Liu, Z.; Pourpoint, F.; Armstrong, A. R.; Grey, C. P.; Bruce, P. G. *Angew. Chem., Int. Ed.* **2012**, *51*, 2164.
(28) Liu, S.; Jia, H.; Han, L.; Wang, J.; Gao, P.; Xu, D.; Yang, J.; Che, S. *Adv. Mater.* **2012**, *24*, 3201.
(29) Wang, W.; Sa, Q.; Chen, J.; Wang, Y.; Jung, H.; Yin, Y. *ACS Appl. Mater. Interfaces* **2013**, *5*, 6478.
(30) Yang, S.; Cai, Y.; Cheng, Y.; Varanasi, C. V.; Liu, J. *J. Power Sources* **2012**, *218*, 140.
(31) Cheng, Y.; Zhang, H.; Varanasi, C. V.; Liu, J. *Sci. Rep.* **2013**, *3*, 3195.
(32) Cheng, Y.; Liu, J. *Mater. Res. Lett.* **2013**, *1*, 175.
(33) Li, J.; Liu, K.; Liang, S.; Zhou, W.; Pierce, M.; Wang, F.; Peng, L.; Liu, J. *ACS Nano* **2013**, *8*, 554.